Accelerating EMT Studies by Merging Interconnected Transmission Lines with Applications in Protection and Stability Analysis

Nasib Khadka and Reza Jalilzadeh Hamidi

August 24, 2026

Accelerating EMT Studies by Merging Interconnected Transmission Lines with Applications in Protection and Stability Analysis

Nasib Khadka, IEEE, Student Member
Georgia Southern University
Department of ECE
Statesboro, Georgia, USA
nasibkhadka99@gmail.com

Reza Jalilzadeh Hamidi, IEEE, Senior Member
Georgia Southern University
Department of ECE
Statesboro, Georgia, USA
rhamidi@georgiasouthern.edu

***Abstract*—With the penetration of inverter-based resources in power grids, phasor-domain analysis (RMS analysis) is becoming less effective, and the demand for Electromagnetic Transient (EMT) analysis is growing. However, EMT analysis is computationally intensive, particularly for large-scale grids when a small simulation timestep is required. One of the grid components that limits the maximum allowable timestep is the Transmission Line (TL). Among different TL models, the Bergeron TL model is widely used in EMT studies on grid dynamics and protection. However, it restricts the maximum simulation timestep to the shortest propagation delay of the TLs in the grid. This paper proposes a mathematical method for merging the Bergeron models of interconnected TLs (i.e., TLs connected to a common bus) to allow the use of a simulation timestep up to twice the minimum propagation delay. This increases the speed of EMT simulations. The proposed model is evaluated using EMTP-RV. The results demonstrate that the proposed model enhances the simulation speed by nearly 41% for the test cases. However, the error in the results remains smaller than 2.1% in the test cases.**

***Keywords*—Bergeron model, computational burden, EMT, model reduction, transmission line.**

I. INTRODUCTION

Integration of Inverter-Based Resources (IBRs) to electric grids adds fast dynamics to the behavior of grids. This challenges the accuracy of the conventional phasor-domain or RMS analysis. Therefore, the demand for Electromagnetic Transient (EMT) solutions is rising [1]. However, the computational burden of EMT analysis is substantial. Consequently, researchers have proposed the following primary approaches to accelerate EMT analysis: i) hybrid EMT-RMS co-simulation [2], [3], ii) parallel processing [4], [5], iii) multirate simulation [6], [7], iv) Average-Value Models (AVM) [8], [9], and v) model reduction [10-14]. In the following, these approaches are briefly reviewed, and the closest methods to the proposed one are elaborated.

In hybrid EMT-RMS co-simulations, the grid is divided into a detailed system (EMT network) and an external system (electromechanical network), which are respectively solved using the EMT and RMS analyses [2]. However, delays in exchanging data between these two networks can result in numerical stability issues [3], [15]. Another challenge is the continuous expansion of EMT networks by the addition of IBRs [1], [2] that reduces the speed of the EMT simulation.

In parallel processing [4], the grid is first decomposed into smaller subnetworks (coarse-grained) utilizing delay elements. Subsequently, the subnetworks are analyzed in parallel by separate processing units. Transmission Lines (TLs) are usually used as the delay element in the coarse-grained decomposition due to their natural propagation delay, which is referred to as line-interfacing [16]. However, the number, location, and length of TLs influence the performance of parallel processing. In particular, the maximum simulation timestep (Δt) is limited by TL propagation delays [17]. While adding artificial delay elements or latency buffers can provide the required delay for partitioning [5], it can increase the error in simulation results [7]. Moreover, parallel processing requires expensive computational resources.

Following the multirate approach, while all areas of a large grid are analyzed by EMT solutions, different timesteps are utilized for these areas to reduce the computational burden. For example, in [6], the grid is divided into three areas, namely the power-electronic, main, and remote areas. Then, the following timesteps are respectively considered for them: substep (smallest Δt), main timestep, and superstep (largest Δt). However, interfacing several different areas can be challenging or may introduce cumulative errors [7], [18].

AVMs are developed by representing semiconductor switches with canonical switching cells [19]. This removes high-frequency power-electronic switching, which requires small timesteps. Therefore, AVMs permit the use of larger timesteps to improve the speed of EMT simulations. However, the possible delays in interfacing AVMs and the rest of the system can lead to numerical inaccuracies or instabilities [9].

Model reduction broadly refers to retaining the input-output behavior of a system while reducing its internal complexity to decrease the computational burden. As for the applications of reduced models in EMT simulation, Frequency-Dependent Network Equivalents (FDNEs) are well-known to approximate a part of a grid with a rational transfer function [10]. However, accuracy issues are reported in [20], and it is concluded that the number of poles should be considerably high to achieve a precise fitting function in some cases. Additionally, curve-fitting issues in finding the transfer function challenge the use of FDNEs [21]. However, reduced models tailored for specific components are proposed to increase the speed of EMT simulation. In [11], a reduced model is introduced for converter simulations. In [12], [13], the reduced models for power-electronic transformers and

This material is based upon work supported by the National Science Foundation under Award No. 2501854.

HVDC links are respectively addressed. In [14], several reduced models of grid-tied inverters are discussed and compared. While TLs form a major portion of transmission grids, to the best of our knowledge, no reduced model for interconnected TLs that preserves propagation delays has been reported in the literature.

The inspiration for this work is the lack of reduced models for representing interconnected TLs to accelerate EMT analysis. The contribution of this paper is to introduce a reduced, but high-fidelity, model for representing interconnected TLs that share a common bus. While the frequency-dependent [22] and universal line models [23] take frequency-dependent features of TLs into account, their computational burdens are significantly higher compared to the Bergeron model [24]. Therefore, the Bergeron model is often preferred in EMT studies requiring long simulation times and focusing on the main frequency, such as protection and stability studies [25], [26], [27], [28]. The importance of the proposed method is that it can reduce the computational burden of EMT-type simulations.

The proposed method mathematically removes the common bus between the TLs (Bus c in Figs. 1(a) and (b)) and merges the Bergeron models of interconnected TLs into a multiterminal component that can replace the original lines, as shown in Fig. 1(c). By removing the common bus, the maximum allowable Δt can increase from the minimum propagation delay of TLs to twice that value.

The main advantage of the proposed method is its high fidelity, as it retains the propagation delays between the terminals of the interconnected TLs (k buses in Fig. 1). Additionally, the proposed method does not encounter curve-fitting issues in FDNE, as it follows closed-form solutions mainly based on substitution. The performance of the proposed method is evaluated through several scenarios with switching events. The results confirm the ability of the proposed method to improve the speed of EMT simulations while maintaining accuracy.

II. Proposed Method

A. Methodology

It is common in the literature to develop line models first for single-phase TLs, and then extend the model to multi-phase lines [24], [29]. Similarly, the proposed method is explained using an example consisting of two single-phase TLs sharing the common Bus c, as shown in Fig. 1(a). However, the developed formulations support any number of TLs. The end terminals of TL1 are Buses k_1 and m_1, and its characteristic impedance and propagation delay are z_1 and τ_1, respectively. Likewise, TL2 connects Buses k_2 and m_2, and its parameters are z_2 and τ_2. The Bergeron model of these TLs is shown in Fig. 1(b), and their defining equations are as follows [24]:

$$\begin{cases} i_{km_j}(t) = e_{k_j}(t)y_j + i_{k_j}(t) & (1.1) \\ i_{mk_j}(t) = e_{m_j}(t)y_j + i_{m_j}(t) & (1.2) \\ i_{k_j}(t) = -e_{m_j}(t-\tau_j)y_j - i_{mk_j}(t-\tau_j) & (1.3) \\ i_{m_j}(t) = -e_{k_j}(t-\tau_j)y_j - i_{km_j}(t-\tau_j) & (1.4) \end{cases}$$

where j belongs to the set $N = \{1,2,3,\dots,n\}$ in which n is the

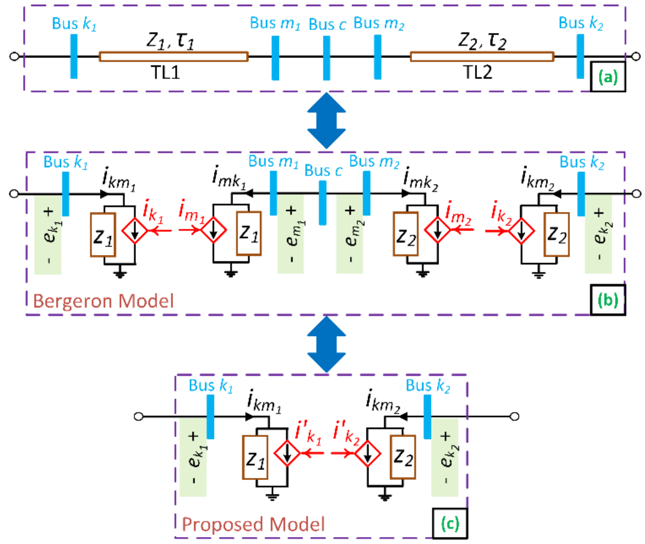

Fig. 1. (a) Interconnected TLs. (b) The Bergeron model. (c) The proposed model.

total number of interconnected TLs sharing the common Bus. Referring to Fig. 1(b), i_{km_j} is the current flowing from Bus k_j to Bus m_j of TL j, and i_{mk_j} is the current flowing reversely from Bus m_j to Bus k_j. y_j is the characteristic admittance of TL j, τ_j is the TL's propagation delay, e_{k_j} and e_{m_j} are the voltages of Buses k_j and m_j, and i_{k_j} and i_{m_j} are the history currents.

With reference to the Bergeron model shown in Fig. 1(b), the buses connected to the common Bus c are considered m-buses. Therefore, their voltages are the same. This can be formulated as $e_{m_1}(t) = e_{m_2}(t) = \cdots = e_{m_n}(t) = e_c(t)$ where $e_c(t)$ is the voltage of the common bus. Concurrently, the KCL at Bus c suggests

$$i_{mk_1}(t) + i_{mk_2}(t) + \cdots + i_{mk_n}(t) = 0 \tag{2}$$

Replacing $i_{mk_j}, \forall j = 1,2,..,n$ with their equivalents given in (1.2) and using e_c instead of the voltage of m-buses (i.e., $e_{m_j}(t) = e_c(t), \forall j = 1,2,\dots,n$), (2) can be written as

$$e_c(t)\sum_{j=1}^{n} y_j + \sum_{j=1}^{n} i_{m_j}(t) = 0 \tag{3}$$

Defining $Y \coloneqq \sum_{j=1}^{n} y_j$ and replacing i_{m_j} in (3) with its equivalent given in (1.4) result in

$$e_c(t)Y - \sum_{j=1}^{n}\left(e_{k_j}(t-\tau_j)y_j + i_{km_j}(t-\tau_j)\right) = 0 \tag{4}$$

Solving (4) for $e_c(t)$ leads to (5), which is a function of the voltages and currents of k-buses (i.e., outer buses).

$$e_c(t) = Y^{-1}\sum_{j=1}^{n}\left(e_{k_j}(t-\tau_j)y_j + i_{km_j}(t-\tau_j)\right) \tag{5}$$

Therefore, the voltage of the common Bus c can be determined only using the voltages and currents of the outer buses.

Let us refer to any of the interconnected lines with subscript p. Therefore, based on (3), the history current of any TL p is i_{m_p}, which can be expressed as (6).

$$i_{m_p}(t) = -e_c(t)\sum_{j=1}^{n} y_j - \sum_{j=1, j\neq p}^{n} i_{m_j}(t) \tag{6}$$

Using the definition of Y and replacing i_{m_j} in (6) with its equivalent provided in (1.4) yield

$$i_{m_p}(t) = -e_c(t)Y + \sum_{j=1, j\neq p}^{n} \left(e_{k_j}(t-\tau_j)y_j + i_{km_j}(t-\tau_j)\right) \tag{7}$$

Therefore, the history current at the inner buses (m-buses) is a function of the voltages and currents of only k-buses. Referring to (1.3) and Fig. 1(b), i_k represents the history current at the outer buses (k-buses). But it is a function of the inner bus voltages and currents (i.e., e_m and i_{mk}) and must be expressed in terms of outer bus parameters. As all e_m equal e_c, and i_{mk} can be replaced with (1.2) for any TL p, $i_{k_p}(t)$ is

$$i_{k_p}(t) = -e_c(t-\tau_p)y_p - e_c(t-\tau_p)y_p - i_{m_p}(t-\tau_p) \tag{8}$$

which is simplified as

$$i_{k_p}(t) = -2e_c(t-\tau_p)y_p - i_{m_p}(t-\tau_p) \tag{9}$$

Replacing $i_{m_p}(t-\tau_p)$ in (9) with respect to (7), and defining $\tau_{pj} := \tau_p + \tau_j$, $i_{k_p}(t)$ is expressed as

$$i_{k_p}(t) = -2e_c(t-\tau_p)y_p + e_c(t-\tau_p)Y - \sum_{j=1, j\neq p}^{n} \left(e_{k_j}(t-\tau_{pj})y_j + i_{km_j}(t-\tau_{pj})\right) \tag{10}$$

which is equal to

$$i_{k_p}(t) = (-2y_p + Y)e_c(t-\tau_p) - \sum_{j=1, j\neq p}^{n} \left(e_{k_j}(t-\tau_{pj})y_j + i_{km_j}(t-\tau_{pj})\right) \tag{11}$$

Then, replacing $e_c(t-\tau_p)$ in (11) with respect to (5) results in

$$\begin{aligned} i_{k_p}(t) = & -2y_pY^{-1}\sum_{j=1}^{n} \left(e_{k_j}(t-\tau_{pj})y_j + i_{km_j}(t-\tau_{pj})\right) \\ & + \sum_{j=1}^{n} \left(e_{k_j}(t-\tau_{pj})y_j + i_{km_j}(t-\tau_{pj})\right) \\ & - \sum_{j=1, j\neq p}^{n} \left(e_{k_j}(t-\tau_{pj})y_j + i_{km_j}(t-\tau_{pj})\right) \end{aligned} \tag{12}$$

It is based on the voltages and currents of k-buses only. By defining

$$\begin{cases} \alpha_{pj}(t) := e_{k_j}(t-\tau_{pj})y_j + i_{km_j}(t-\tau_{pj}), \forall j = 1,2,\ldots,n \\ \alpha_{pp}(t) := e_{k_p}(t-\tau_{pp})y_p + i_{km_p}(t-\tau_{pp}), if\ j = p \end{cases} \tag{13}$$

Then, (12) can be written in the following short form.

$$i'_{k_p}(t) = -\left(2y_pY^{-1}\sum_{j=1}^{n} \left(\alpha_{pj}(t)\right)\right) + \alpha_{pp}(t) \tag{14}$$

where i'_{k_p} denotes history currents connected to k-buses, as shown in Fig. 1(c). Accordingly, and with respect to Fig. 1(c), the multiterminal component representing the TLs only requires the parameters of k-buses, comprising e_k, i_{km}, and i'_k.

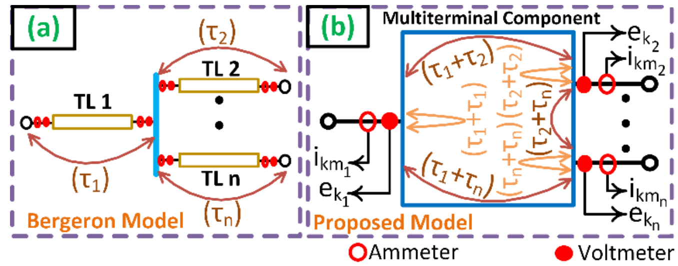

Fig. 2. Propagation delays of (a) the Bergeron and (b) proposed models.

The set of equations defining the multiterminal component is given in (15). It should be noted that p refers to a particular TL in the set of n interconnected TLs.

$$\begin{cases} i'_{k_p}(t) = -\left(2y_pY^{-1}\sum_{j=1}^{n} \left(\alpha_{pj}(t)\right)\right) + \alpha_{pp}(t) \\ i_{km_p}(t) = e_{k_p}(t)y_p + i'_{k_p}(t) \end{cases}. \tag{15}$$

B. Discussion on Propagation Delays

The propagation delays between the terminals of the Bergeron and proposed models are shown in Fig. 2. For any TL p in the set of n interconnected TLs, the Bergeron model uses the terminal-to-terminal delay τ_p to compute the history currents (i.e., i_{k_p} and i_{m_p}) according to (1.3) and (1.4). However, the proposed model computes the history current (i.e., i'_{k_p} in (14)) using the delays between the outer terminals τ_{pj}, where τ_{pj} is the sum of the propagation delays of TL p (i.e., τ_p) and TL j (i.e., τ_j), for all $j = 1,2,\ldots,n$, including $j = p$ that results in τ_{pp}. Therefore, the minimum propagation delay in the multiterminal component is twice the lowest propagation delay of TLs. In other words, if τ_{min} is the shortest propagation delay among the interconnected TLs (i.e., $\tau_{min} = \min\{\tau_1, \tau_2, \ldots, \tau_n\}$) the shortest delay in the multiterminal component is $\tau_{min} + \tau_{min} = 2\tau_{min}$, which is the sum of the traveling time of a wave from the outer bus of the corresponding line to the common bus and its return to the same outer bus.

Therefore, the proposed method enables the selection of a maximum timestep (Δt) for the EMT analysis twice τ_{min} (i.e., $0 < \Delta t \leq 2\tau_{min}$), while the Bergeron model necessitates that $0 < \Delta t \leq \tau_{min}$.

C. Implementation in EMT Simulations

The implementation of the proposed model in EMT simulators is presented in Algorithm 1. This algorithm is executed at the beginning of each simulation timestep to update all history currents. For example, as the multiterminal component shown in Fig. 1(c) has two terminals, the algorithm is executed for $p = 1$ and $p = 2$ to determine i'_{k_1} and i'_{k_2}. Then, the simulator analyzes the grid for one Δt. While the algorithm is self-descriptive, it is explained as follows:

In the initialization stage, the necessary constants are determined. In Line 1, the proposed method receives the simulation parameters. In Line 2, all terminal-to-terminal propagation delays, including τ_{pp}, are calculated. None of them should be smaller than Δt, which is checked in Line 3. The sum of the characteristic admittances is used repeatedly in the rest of

Algorithm 1: Implementation of the proposed model in EMT simulators.

Initialization:

1. $n \leftarrow$ Number of TLs; $\Delta t \leftarrow$ Simulation timestep; $T \leftarrow$ Total simulation time
2. $\tau_{pj} \leftarrow \tau_p + \tau_j, \forall j = 1, 2, \ldots, n$
3. **If** $\tau_{pj} < \Delta t, \forall j = 1, 2, \ldots, n$; **Stop** // Δt cannot be larger than any τ_{pj} //
4. $\Upsilon \leftarrow \sum_{j=1}^{n} y_j$

Computing history terms:

5. **For** $j = 1, 2, \ldots, n$
6. **If** (**Remainder** $(\tau_{pj}/\Delta t) \neq 0$) // τ_{pj} is not an integer multiple of Δt //
7. $f_{pj} \leftarrow \lfloor \tau_{pj}/\Delta t \rfloor$ // $\lfloor . \rfloor$ is the floor function. //
8. $t_a \leftarrow t - (f_{pj} + 1)\,\Delta t$
9. $t_b \leftarrow t - f_{pj}\,\Delta t$
10. $e_{k_j}(t - \tau_{pj}) \leftarrow$ **Interpolate** $\left(e_{k_j}(t_a), e_{k_j}(t_b)\right)$
11. $i_{km_j}(t - \tau_{pj}) \leftarrow$ **Interpolate** $\left(i_{km_j}(t_a), i_{km_j}(t_b)\right)$
12. **Endif**
13. $\alpha_{pj}(t) \leftarrow e_{k_j}(t - \tau_{pj}) y_j + i_{km_j}(t - \tau_{pj})$ // Refer to (13) //
14. **If** $j = p$
15. $\alpha_{pp}(t) \leftarrow e_{k_p}(t - \tau_{pp}) y_p + i_{km_p}(t - \tau_{pp})$ // Refer to (13) //
16. **Endif**
17. **Endfor**
18. $i'_{k_p}(t) \leftarrow -\left(2 y_p \Upsilon^{-1} \sum_{j=1}^{n} (\alpha_{pj}(t))\right) + \alpha_{pp}(t)$ //Refer to (14) //

the algorithm. Therefore, calculating and recording it accelerates the calculations, which are carried out in Line 4.

The loop defined in Line 5 contains Lines 6 to 16 and executes them for all $j = 1, 2, \ldots, n$. In Line 6, it is evaluated whether each terminal-to-terminal propagation delay, including τ_{pp}, is an integer multiple of Δt. If it is not, the values of e_{k_j} and i_{km_j} are obtained by interpolating the recorded history values through Lines 7 to 11 [29]. In Lines 13 and 15, α_{pj} and α_{pp} are calculated. Finally, the history current $i'_{k_p}(t)$ is calculated in Line 18. This algorithm should be called for every single terminal of the multiterminal component. When all the history currents are determined, the simulator can analyze the grid for one iteration.

III. Test Cases, Results, and Discussion

The test case is shown in Fig. 3. It includes two 345-kV TLs that are interconnected at the common Bus c. The characteristic impedances of the TLs are $z_1 = 400\ \Omega$ and $z_2 = 350\ \Omega$ [30], and their propagation delays are $\tau_1 = 300$ µs and $\tau_2 = 100$ µs. One phase of an ideal, 60-Hz, 345-kV voltage source is connected to TL1 via a series one-ohm resistor, since the proposed model is single phase in accordance with the tradition in explaining TL models [24], [29]. The source impedance is retained low to increase the fault currents, which magnifies the errors in the results. The impedance of the load is 120+j120 Ω. This also results in the flow of higher currents that intensifies the probable inaccuracies of the proposed model. The voltage meters (1 and 2 in Fig. 3) and current meters (3 and 4 in Fig. 3) are located at the outer ends of the TLs (k-buses).

Both the Bergeron and proposed models of the test system are implemented in EMTP-RV. A simulation timestep of 100 µs is selected for the Bergeron model, but it is 200 µs for the proposed model, which are both the maximum allowable timesteps. The employed numerical solver is the trapezoidal rule of integration. The total simulation length is 100 s that contains

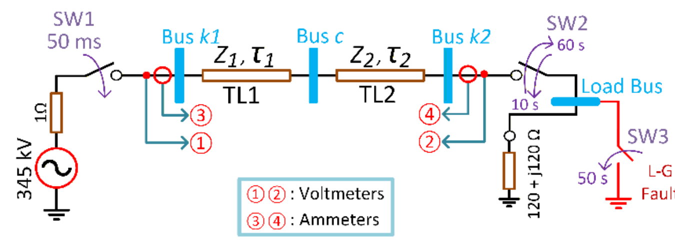

Fig. 3. Test case.

four sequential scenarios.

The performance of the proposed model is assessed in four scenarios by comparing its results with the results of the Bergeron model. The relative errors are calculated by

$$\text{Error}\ \% = |x_P - x_B| / x_B \times 100 \qquad (16)$$

where x_P and x_B represent currents or voltages calculated by the proposed and Bergeron models, respectively. For each scenario, the maximum relative error is identified and reported in Table I. Additionally, the results from both models are observed along the time axis for e_{k_1}, e_{k_2}, i_{km_1}, and i_{km_2}. However, due to the space limitation, only the voltage waveform at Bus k_2 is shown in Fig. 4, as it carries more information than the other measurements.

A. Scenario 1: Line Energization

With reference to Fig. 3, the TLs are initially unenergized. However, to energize the TLs, SW1 is closed at $t = 50$ ms, while SW2 remains disconnected (i.e., Bus k_2 is open-circuited). This scenario continues until $t = 10$ s. The relative error is calculated at each timestep using (16), and its maximum is reported in Table I.

The voltage of Bus k_1 is denoted with e_{k_1}, and its location is shown in Fig. 3 with 1. The maximum difference in e_{k_1} computed by the models occurs at $t = 1.3116$ s, where e_B and e_P are almost identical and approximately equal to 93.8574 kV. Consequently, the corresponding relative error is negligible as reported in Table I. The voltage of Bus k_2 is denoted with e_{k_2} (2 in Fig. 3). As shown in Fig. 4(a), both models find the voltage zero before the closing of SW1. However, 400 µs after the switching (i.e., $t = 50.4$ ms), e_{k_2} sharply increases by the arrival of the first traveling wave. The results of both models are identical, as can be observed in Fig. 4(a). The maximum difference occurs at $t = 1.3112$ s, where both e_B and e_P are nearly 134.4996 kV. Therefore, the maximum relative error in e_{k_2} is negligible, as given in Table I. The maximum error in i_{km_1} (3 in Fig. 3) is detected at $t = 1.3116$ s, where both i_B and i_P are 105.0703 A. Therefore, the maximum relative error is negligible. As for i_{km_2} (4 in Fig. 3), since Bus k_2 is open-circuited, i_{km_2} is zero throughout the first scenario. Thus, the relative error cannot be defined, as it implies division by zero.

B. Scenario 2: Line Loading

This scenario starts by closing SW2 at $t = 10$ s to connect the load to Bus k_2, as depicted in Fig. 3, and finishes at $t = 50$ s. The results of the Bergeron and proposed models are compared at each timestep, and the maximum relative errors are reported in Table I.

TABLE I. MAXIMUM RELATIVE ERRORS

Parameter	Relative Error (%)			
	Scenario 1	Scenario 2	Scenario 3	Scenario 4
e_{k_1} at ①	≈ 0	0.0087	0.0004	≈ 0
e_{k_2} at ②	≈ 0	0.7515	Undefined[a]	≈ 0
i_{km_1} at ③	≈ 0	2.0422	0.0021	≈ 0
i_{km_2} at ④	Undefined[a]	1.3859	0.0021	Undefined[a]

[a] Both $|x_P|$ and $|x_B|$ equal zero, leading to 0/0, which is undefined.

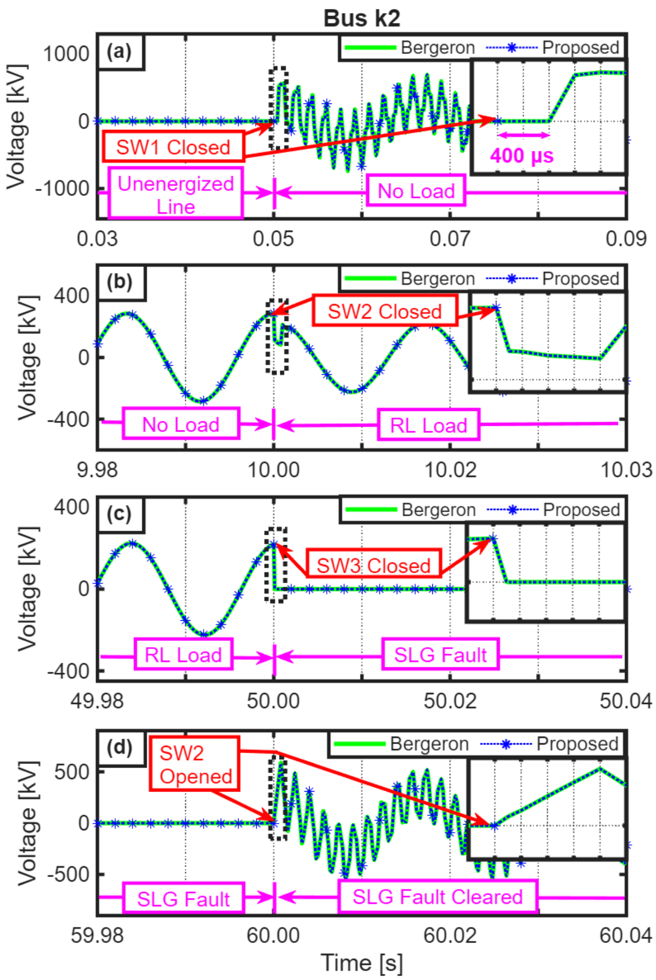

Fig. 4. Voltage waveforms at Bus k_2 (a) Scenario 1 (b) Scenario 2 (c) Scenario 3 (d) Scenario 4.

The maximum difference between the two models in finding e_{k_1} occurs at $t = 10.0054$ s where e_B =-126.8474 kV (by the Bergeron model) and e_P = -126.8363 kV (by the proposed model). This leads to a relative error of 0.0087%, as given in Table I. The maximum relative error of e_{k_2} is at t =10.0012 s, where e_B = 198.5880 kV and e_P = 200.0804 kV, which results in a relative error of 0.7515%. The waveforms of e_{k_2} obtained by both models are depicted in Fig. 4(b). As it is obvious in the figure, before closing SW2 at $t = 10$ s, the voltage is in the steady state. However, by connecting the load, the voltage drops after a short transient. It is clear in Fig. 4(b) that the results of both the Bergeron and proposed models are almost identical. Similarly, the maximum relative error in i_{km_1} is detected at t = 10.0054 s, which is 2.0422% based on i_B = 541.7327 A and i_P = 530.6697 A. In addition, the load-side current i_{km_2} is measured as i_B = -798.1631 A and i_P = -787.1013 A at t = 10.0050 s that result in the maximum relative error of 1.3859%.

C. Scenario 3: Single-Line-to-Ground Fault

This scenario (from $t = 50$ s to $t = 60$ s) studies the performance of the proposed model in case of faults. As shown in Fig. 3, a solid Single-Line-to-Ground (SLG) fault is applied to Bus k_2 by closing SW3 at $t = 50$ s.

At t =50.0038 s, e_B = 33.0096 kV and e_P = 33.0095 kV that result in the maximum relative error of 0.0004% in e_{k_1}. However, $e_{k_2} = 0$ throughout Scenario 3, and the relative error cannot be defined. The waveform of e_{k_2} obtained by both models are depicted in Fig. 4(c). It can be observed that the voltage e_{k_2} drops to zero with the inception of the SLG fault. The maximum relative error in i_{km_1} is detected at t = 50.0038 s, which is 0.0021% based on i_B = 5.8047 kA and i_P = 5.8048 kA. As for i_{km_2}, it is measured as i_B = 5.9391 kA and i_P =5.9392 kA at t = 50.0042 s that results in the maximum relative error of 0.0021%.

D. Scenario 4: SLG Fault Clearing

This scenario starts at $t = 60$ s by opening SW2. At this moment, the SLG fault in the third scenario is cleared as depicted in Fig. 3. The results of the proposed model are compared to the results of the Bergeron model for the next 40 seconds until t = 100 s, and the error at each timestep is determined.

It is found that the maximum error in e_{k_1} occurs at t =79.7680 s, where e_B and e_P are both almost 246.9014 kV. As a result, the relative error is negligible. The waveform of e_{k_2} is depicted in Fig. 4(d). It is clear that the voltage of Bus k_2 is zero before fault clearance. However, after clearing the fault, the voltage e_{k_2} rises again. The maximum relative error in e_{k_2} is found to be negligible. The maximum relative error in i_{km_1} is also negligible, and since Bus k_2 is open-circuited, i_{km_2} is zero throughout Scenario 4. Thus, the relative error cannot be defined.

To compare the computational intensity of the Bergeron and proposed models, all of the four mentioned scenarios (i.e., an entire simulation time of 100 s) are executed ten times for each model. The simulation timesteps are considered the maximum allowed, which are Δt = 100 μs and Δt = 200 μs, respectively, for the Bergeron and proposed models. The simulations are performed by a DELL OPTIPLEX 7060 computer equipped with an Intel i7-8700/3.20 GHz CPU and 64 GB of RAM. The average simulation runtimes of the Bergeron and the proposed models are respectively, 9.27688 s and 5.47578 s. Therefore, the proposed model is 40.97% faster than the Bergeron model in these scenarios.

IV. CONCLUSION

Since EMT-type simulations are computationally intensive, solutions for reducing their computational demand are required. Several methods for increasing the speed of simulations have been proposed in the literature. However, while Transmission Lines (TLs) constitute a large portion of electrical networks, high-fidelity reduced models for a set of interconnected TLs are unavailable. Among different TL models, the Bergeron model has wide applications in dynamic and protection studies where relatively long simulations should be executed, and the fundamental frequency is of interest. Accordingly, this paper proposes a method for merging the Bergeron models of interconnected TLs that share a common bus. The merged TLs are represented with a multiterminal component with the minimum terminal-to-terminal propagation delay twice the shortest propagation delay of TLs.

The proposed model is implemented in EMTP-RV. The results of the Bergeron and proposed models are compared in four different scenarios, including switchings and a fault. The proposed model allows the use of a simulation timestep twice the minimum propagation delay of the TLs, while it is limited to the minimum propagation delay when the Bergeron model is utilized. According to the results, the simulation speed increases by almost 41%, while the maximum relative error does not exceed 2.1% in the tests. However, the proposed method cannot provide the voltages and currents of the common bus. Future work will extend the proposed model to three-phase TLs.

References

[1] NERC, "Electromagnetic transient analysis in operations planning," Atlanta, GA, USA, Jun. 2025. [Online]. Available: https://www.nerc.com/globalassets/our-work/reports/white-papers/whitepaper_-emt-analysis-in-operations_v2.0_final.pdf

[2] Q. Huang and V. Vittal, "Advanced EMT and phasor-domain hybrid simulation with simulation mode switching capability for transmission and distribution systems," *IEEE Trans. Power Syst.*, vol. 33, no. 6, pp. 6298–6308, Nov. 2018, doi: 10.1109/TPWRS.2018.2834561.

[3] D. Rimorov, J. Huang, C. F. Mugombozi, T. Roudier, and I. Kamwa, "Power coupling for transient stability and electromagnetic transient collaborative simulation of power grids," *IEEE Trans. Power Syst.*, vol. 36, no. 6, pp. 5175–5184, Nov. 2021, doi: 10.1109/TPWRS.2021.3075908.

[4] Z. Zhou and V. Dinavahi, "Fine-grained network decomposition for massively parallel electromagnetic transient simulation of large power systems," *IEEE Power Energy Technol. Syst. J.*, vol. 4, no. 3, pp. 51–64, Sep. 2017, doi: 10.1109/JPETS.2017.2732360.

[5] Q. Wang, J. Xu, K. Wang, P. Wu, W. Chen, and Z. Li, "Parallel electromagnetic transient simulation of power systems with a high proportion of renewable energy based on latency insertion method," *IET Renewable Power Gen*, vol. 17, no. 1, pp. 110–123, Jan. 2023, doi: 10.1049/rpg2.12385.

[6] M. Mao, "Superstep simulation," presented at the *2019 China User's Group Meeting-RTDS Technologies Inc.*, Oct. 2019.

[7] D. Shu, X. Xie, Q. Jiang, G. Guo, and K. Wang, "A multirate EMT co-simulation of large AC and MMC-based MTDC systems," *IEEE Trans. Power Syst.*, vol. 33, no. 2, pp. 1252–1263, Mar. 2018, doi: 10.1109/TPWRS.2017.2734690.

[8] S. Chiniforoosh *et al.*, "Definitions and applications of dynamic average models for analysis of power systems," *IEEE Trans. Power Delivery*, vol. 25, no. 4, pp. 2655–2669, Oct. 2010, doi: 10.1109/TPWRD.2010.2043859.

[9] S. Ebrahimi and J. Jatskevich, "Average-value model for voltage-source converters with direct interfacing in EMTP-type solution," *IEEE Trans. Energy Convers.*, vol. 38, no. 3, pp. 2231–2234, Sep. 2023, doi: 10.1109/TEC.2022.3220085.

[10] J. M. Verduzco-Durán, A. Medina-Rios, A. Ramos-Paz, R. Cisneros-Magaña, and J. C. Godinez-Delgado, "Electromagnetic transient analysis using a frequency dependent network equivalent for power systems integrating wind generation sources," in *2024 IEEE Power & Energy Society General Meeting (PESGM)*, Seattle, WA, USA: IEEE, Jul. 2024, pp. 1–5. doi: 10.1109/PESGM51994.2024.10688470.

[11] J. Wang, X. Fu, P. Li, and J. Mahseredjian, "Reduced-order and simultaneous solution of power and control system equations in EMT simulations," *Electric Power Systems Research*, vol. 252, p. 112412, Jan. 2026, doi: 10.1016/j.epsr.2025.112412.

[12] J. Xu *et al.*, "High-speed electromagnetic transient (EMT) equivalent modelling of power electronic transformers," *IEEE Trans. Power Delivery*, vol. 36, no. 2, pp. 975–986, Apr. 2021, doi: 10.1109/TPWRD.2020.2998498.

[13] C. A. Ruiz-Zea *et al.*, "Dual-band reduced-order model of an HVDC link embedded into a power network for EMT studies," *IEEE Trans. Energy Convers.*, vol. 35, no. 1, pp. 416–424, Mar. 2020, doi: 10.1109/TEC.2019.2935892.

[14] K. Sano, S. Horiuchi, and T. Noda, "Comparison and selection of grid-tied inverter models for accurate and efficient EMT simulations," *IEEE Trans. Power Electron.*, vol. 37, no. 3, pp. 3462–3472, Mar. 2022, doi: 10.1109/TPEL.2021.3117633.

[15] V. Jalili-Marandi, V. Dinavahi, K. Strunz, J. A. Martinez, and A. Ramirez, "Interfacing techniques for transient stability and electromagnetic transient programs IEEE Task Force on interfacing techniques for simulation tools," *IEEE Trans. Power Delivery*, vol. 24, no. 4, pp. 2385–2395, Oct. 2009, doi: 10.1109/TPWRD.2008.2002889.

[16] V. Dinavahi and N. Lin, Parallel Dynamic and Transient Simulation of Large-Scale Power Systems: A High Performance Computing Solution. Cham, Switzerland: Springer International Publishing, 2022. doi: 10.1007/978-3-030-86782-9.

[17] M. Xiong *et al.*, "ParaEMT: An open source, parallelizable, and HPC-compatible EMT simulator for large-scale IBR-rich power grids," *IEEE Trans. Power Delivery*, vol. 39, no. 2, pp. 911–921, Apr. 2024, doi: 10.1109/TPWRD.2023.3342715.

[18] H. Wang, J. Xu, and M. Feng, "Multirate EMT simulation of power electronic transformers with high-precision firing signals," *IEEE Trans. Power Delivery*, pp. 1–12, 2026, doi: 10.1109/TPWRD.2026.3656907.

[19] J. G. Kassakian, D. J. Perreault, G. C. Verghese, and M. F. Schlecht, Principles of Power Electronics. Cambridge, UK: Cambridge University Press, 2024.

[20] J. P. L. Salvador, F. C. Neto, C. S. Lima, and K. Strunz, "Accuracy and realization issues in frequency dependent sequence networks," presented at the *IPST 2015*, Cavtat, Croatia: IPST, Jun. 2015.

[21] B. Salarieh and H. M. J. De Silva, "Review and comparison of frequency-domain curve-fitting techniques: Vector fitting, frequency-partitioning fitting, matrix pencil method and loewner matrix," *Electric Power Systems Research*, vol. 196, p. 107254, Jul. 2021, doi: 10.1016/j.epsr.2021.107254.

[22] J. Marti, "Accurate modelling of frequency-dependent transmission lines in electromagnetic transient simulations," *IEEE Trans. Power Appar. Syst.*, vol. PAS-101, no. 1, pp. 147–157, Jan. 1982, doi: 10.1109/TPAS.1982.317332.

[23] A. Morched, B. Gustavsen, and M. Tartibi, "A universal model for accurate calculation of electromagnetic transients on overhead lines and underground cables," *IEEE Trans. Power Delivery*, vol. 14, no. 3, pp. 1032–1038, Jul. 1999, doi: 10.1109/61.772350.

[24] H. Dommel, "Digital computer solution of electromagnetic transients in single-and multiphase networks," *IEEE Trans. on Power Apparatus and Syst.*, vol. PAS-88, no. 4, pp. 388–399, Apr. 1969, doi: 10.1109/TPAS.1969.292459.

[25] IEEE PES, "Modeling and analysis of system transients using digital programs," IEEE, PES-TR7, 1998. Accessed: Mar. 18, 2026. [Online]. Available: https://resourcecenter.ieee-pes.org/publications/technical-reports/pestr7

[26] PSCAD, "Transmission lines and cables." [Online]. Available: https://www.pscad.com/webhelp/PSCAD/Transmission_Lines_and_Cables/Transmission_Lines_and_Cables.htm

[27] OPAL-RT, "Transmission lines and cables." [Online]. Available: https://opal-rt.atlassian.net/wiki/spaces/PDOCHS/pages/150045425/Transmission+Lines+and+Cables

[28] EMTP-RV, "Line/cable data." Jun. 2022. [Online]. Available: https://emtp.com/documents/EMTP-Documentation/doc/linecabledata/linecabledata.pdf

[29] H. Dommel, Electromagnetic Transient Program (EMTP) Theory Book. Portland, Oregon, USA: Bonneville Power Administration, 1987.

[30] J. D. Glover, M. S. Sharma, and T. J. Overby, Power System Analysis and Design. Stamford, Connecticut: Cengage Learning, 2012.